

# Dynamics of Water in Supercooled Aqueous Solutions of Poly(propylene glycol) As Studied by Broadband Dielectric Spectroscopy and Low-Temperature FTIR-ATR Spectroscopy

Lokendra P. Singh,<sup>§</sup> Silvina Cerveny,<sup>\*†</sup> Angel Alegria,<sup>‡,§</sup> and Juan Colmenero<sup>†,‡,§</sup>

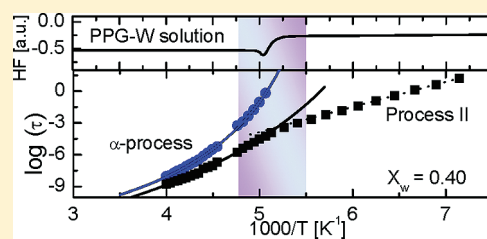
<sup>†</sup>Centro de Fisica de Materiales (CSIC, UPV/EHU)-Materials Physics Center, Paseo Manuel de Lardizabal 5, 20018, San Sebastián, Spain

<sup>‡</sup>Departamento de Física de Materiales, UPV/EHU, Facultad de Química, 20018, San Sebastián, Spain

<sup>§</sup>Donostia International Physics Center, San Sebastián, Spain

 Supporting Information

**ABSTRACT:** Binary water mixtures usually display a water relaxation (process II) which can be studied by broadband dielectric spectroscopy (BDS) at subzero temperatures. In a large collection of binary water mixtures, a slight increase of the relaxation strength is observed for low water concentration, whereas a faster increase is seen above a critical concentration. The assumption behind this result is that at high water concentration self-associations of water molecules are present in the solutions. In this work, we have studied poly(propylene glycol) water solutions by means of broadband dielectric spectroscopy and Fourier transform infrared spectroscopy (FTIR) using the attenuated total reflectance method (ATR) in the temperature range of 120–300 K. By combining both techniques, we found a critical water concentration  $x_w = 0.20$  above which the relaxation strength of the water relaxation (process II) increases more rapidly than at low water concentration indicating the self-association of water molecules.



## INTRODUCTION

At room temperature, liquid water is usually seen as a three-dimensional network of molecules connected by hydrogen bonds, in which water molecules could be tetrahedrally coordinated.<sup>1</sup> Water molecules can make both donor and acceptor hydrogen bonds. This interconnected hydrogen bonding network has been seen as responsible for the anomalous dynamics and structure of bulk water.<sup>2</sup> Below the homogeneous nucleation temperature (230 K), studies of liquid water are more difficult since the crystallization cannot be avoided. Therefore, one of the strategies to study water in its supercooled state is to prepare water solutions (with polymer or biopolymer solutes). This makes it possible to avoid crystallization and study behavior of water molecules at temperatures lower than 230 K. In addition, by studying water solutions, it is also possible to analyze both the interactions between the water molecules and the solute as well as the role of the hydrogen bonds in the structure of solute water.

Previously, we have studied the behavior of several water solutions by broadband dielectric spectroscopy, which is an adequate technique to analyze the orientational dynamical behavior of water molecules on a broad frequency and temperature range due to the big dipolar moment of water molecules.<sup>3</sup> Also, in the literature a lot of attention has been paid to the dielectric behavior of water dynamics in several aqueous mixtures such as carbohydrates,<sup>4–7</sup> proteins,<sup>8–11</sup> and polymers.<sup>12–20</sup> By dielectric spectroscopy, two relaxation processes [called slower process (I) and faster process (II)] are observed at different water concentrations (below the crystallization threshold).<sup>3</sup> Process I is

related with the structural relaxation of the solution (solvent and solute). Its relaxation times follow a typical Vogel–Fulcher–Tammann (VFT)<sup>21</sup> temperature dependence. The characteristics of this process are quite similar to those revealed by the well-known  $\alpha$ -relaxation, which is observed in supercooled liquids and plastic crystals<sup>22–26</sup> above the glass transition temperature ( $T_g$ ). On the other hand, the faster process II observed in these solutions was associated mainly with the relaxation of water molecules. This relaxation (process II) shares several properties in all the different studied solutions (synthetic polymers, small organic molecules, and biopolymers) as well as in hard confinements such as zeolites,<sup>27</sup> MCM-41,<sup>28</sup> or graphite oxide.<sup>29</sup> Further, the loss permittivity ( $\epsilon''$ ) vs  $\log$  (frequency) is symmetric in the whole temperature range, and the temperature dependence of its relaxation times is Arrhenius-like below the glass transition of the hydrated systems.<sup>3,19</sup> It was also pointed out that the relaxation time also follows a general exponential dependence on the weight fraction of water.<sup>20</sup>

Additionally, at certain water concentration,  $x_w$  (for instance,  $x_{\text{critic}} \approx 0.30$  for synthetic polymers and  $x_{\text{critic}} \approx 0.20$  for sugar solutions or for water confined in graphite oxide), the relaxation strengths of process II increase more rapidly than at low water concentration, and the activation energy reaches a value of  $(0.54 \pm 0.04)$  eV.<sup>3,19</sup> Despite the fact that water in these systems is in

**Received:** August 2, 2011

**Revised:** September 29, 2011

**Published:** October 11, 2011

principle surrounded by different environments and different molecular interactions between water and solute should take place, this water relaxation process is almost the same for all systems investigated both below and above the glass transition temperature of the system. This result suggests that at high water concentration self-association of water molecules (clusters) is present in the solutions (at  $x_w > x_{\text{critic}}$ ). However, there are no studies which probe this suggestion for water solutions.

ATR-FTIR spectroscopy is a powerful tool for the analysis of the local structure such as hydrogen bonding. The analysis of the intramolecular OH-stretching mode is one of the methods for probing indirectly the intramolecular network of water since this contribution is sensitive to the level of interaction of the molecule with its surroundings.<sup>30</sup> The main advantage of the ATR technique is that the spectra obtained are free from saturation artifacts,<sup>31</sup> a major problem when studying water by infrared spectroscopy. There have been some papers published on the perturbation of the OH-stretching band of water molecules in the bulk phase or in confining environments, but all of which correspond to experiments done at room temperature or in a restricted temperature interval.<sup>32–36</sup> In addition, recently Aksan and co-workers<sup>37–39</sup> studied three aqueous solutions (acetone–, trehalose–, and protein–water solutions) on a wide temperature range to understand the role of solute on the hydrogen bonding of water at cryogenic temperatures. They found that water was not uniformly distributed in aqueous solutions but formed hydrogen-bonded clusters; i.e., distinct changes in water–water and water–solute hydrogen bonding were identified during supercooling. The observed changes of frequency, intensity, and shape of the IR bands have been interpreted in terms of bound and free water, water clustering,<sup>35,36</sup> water orientation,<sup>37–39</sup> and water networking<sup>27,37–39</sup> on the basis of fitting procedure.

In this work we studied PPG [ $M_n = 425 \text{ g/mol}$ ] and its water mixtures by combining dielectric, calorimetric, and ATR-FTIR techniques at low temperatures. In this way, by means of this combination we are able to clarify at which concentration of water, water–water interaction starts and how H-bonding of water molecules is influenced by the concentration of PPG in solution.

## EXPERIMENTAL SECTION

Polypropylene glycol (PPG) [ $M_n = 425 \text{ g/mol}$ ] from Aldrich Chemical Co., Inc. was used in this study to prepare aqueous solutions with different concentrations. The water used in the study was High-Performance Liquid Chromatography (HPLC) quality from Merck Germany. Aqueous PPG solutions were prepared varying the water concentration from  $0 \leq x_w \leq 0.40$  ( $x_w$  expressed as weight of water over weight of total solution). The bottles with the different solutions were sealed and put in an ultrasonic bath for 40 min to ensure a good microdispersion and homogeneity at molecular level. A broadband dielectric spectrometer, Novocontrol alpha analyzer, was used to measure the complex dielectric function,  $\epsilon^*(\omega)$ ,  $\omega = 2\pi f$ , in the frequency ( $f$ ) range of  $10^{-2}–10^6 \text{ Hz}$ . The solutions were placed between parallel gold-plated electrodes with a diameter of 30 mm, and Teflon spacers of 0.1 mm were used to define the thickness. After cooling at a rate of 10 K/min, isothermal frequency scans recording  $\epsilon^*(\omega)$  were performed every 5 K over the temperature range of 120–285 K. The sample temperature was controlled with stability better than  $\pm 0.1 \text{ K}$ . In addition, the same sample

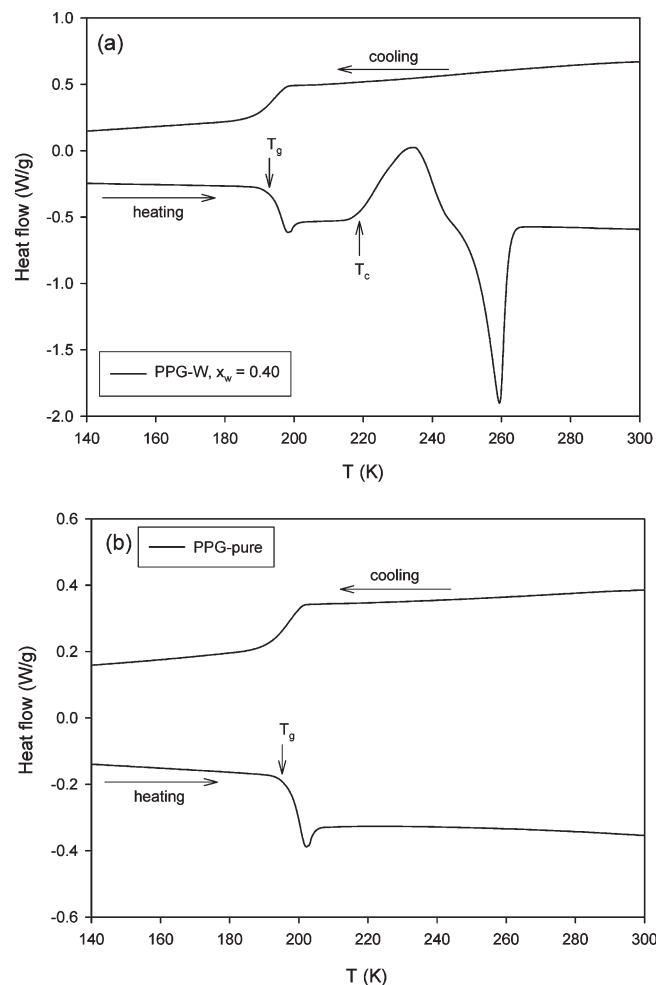


**Figure 1.** (A) Heat flow measured by DSC during cooling (upper curve) and heating (lower curve) at a rate of 10 K/min of PPG–water solution with  $x_w = 0.40$ . A cold crystallization is observed in the temperature range 220–245 K.  $T_g$  and  $T_c$  represent the onset of glass transition temperature and crystallization temperature, respectively. (B) Heat flow measured by DSC during cooling (upper curve) and heating (lower curve) at a rate of 10 K/min of dry PPG.

was measured also in a higher-frequency range  $10^6–10^9 \text{ Hz}$  by using an Agilent radio frequency impedance analyzer 4192B. In this case, parallel gold-plated electrodes with a diameter of 10 mm were used. The most used expression to fit the dielectric spectra in the frequency domain is the Havriliak–Negami (HN) function given as<sup>40</sup>

$$\epsilon^*(\omega) = \epsilon'(\omega) - i\epsilon''(\omega) = \epsilon_\infty + \frac{\Delta\epsilon}{[1 + (i\omega\tau)]^\gamma} \quad (1)$$

where  $\Delta\epsilon$  is the relaxation strength;  $\tau$  is the HN relaxation time;  $\alpha$  and  $\gamma$  represent symmetric and asymmetric broadenings of the loss curve ( $\alpha > 0, \alpha\gamma \leq 1$ ); and  $\epsilon_\infty$  is the high-frequency limit of the real part of permittivity. A particular case of this equation is the Cole–Cole (CC) function, and it is obtained by setting  $\gamma = 1$  in eq 1. In the present case, we chose eq 1 to fit the primary relaxation data for PPG and PPG–water solution (called in this work  $\alpha$ -process), whereas the two sub- $T_g$  processes [called  $\beta$ - and  $\gamma$ -processes for dry PPG and processes II and  $\gamma$ - for water solutions] were fitted by a CC function.

**Table 1.** Details of Equations 3 and 4 for the  $\alpha$ -Process of the PPG–Water Binary System

weight fraction of water ( $x_w$ )	$n_w$	$\log \tau_o$ [s]	$T_0$ [K]	$B$ [K]	fragility index ( $m$ )	$T_{g,100s}$ [K]	$T_{g(dsc)}$ [K]
0.00	0.00	−14.70	149.9	1752.2	71.5	195.7	199.0 ± 1.5
0.02	0.48	−14.41	151.3	1669.3	72.8	195.4	199.0 ± 1.5
0.05	1.24	−14.23	152.7	1582.7	73.2	195.4	198.0 ± 1.5
0.10	2.62	−14.84	149.8	1749.5	72.8	194.9	197.0 ± 1.5
0.20	5.90	−13.62	157.2	1340.7	81.7	194.4	196.0 ± 1.5
0.30	10.11	−14.35	155.2	1431.9	83.2	193.2	195.0 ± 1.5
0.40	15.75	−14.29	155.9	1349.2	87.6	191.7	193.0 ± 1.5

A differential scanning calorimeter (Q2000 TA) was used to measure the thermal response. Standard calorimetric measurements were performed using cooling and heating rates of 10 K/min. Hermetic aluminum pans were used for all the materials. The sample weights were about 15 mg.

Finally, Fourier transform infrared spectroscopy (FTIR) was carried out by means of a JASCO 6500 spectrometer using the attenuated total reflectance method (ATR) in the range of 4500–1000 cm<sup>−1</sup> and in the temperature range 143–298 K. The samples were put in a Golden Gate diamond ATR system. In ATR measurements, the liquid sample is placed in contact through the pipet with the totally reflecting surface of the ATR crystal and pressed by a diamond piston. In this way, a well-defined layer of the sample is obtained. In this configuration, the evanescent wave will be attenuated in regions of the IR spectrum where the sample absorbs energy. The spectra were recorded with a resolution of 4 cm<sup>−1</sup>, by adding 30 repetitive scans to obtain a good signal-to-noise ratio and highly reproducible spectra. The spectra were baseline corrected by using the software spectra analysis from Jasco, and no smoothing of the data was done. The FTIR-ATR spectra of the −OH stretching region were analyzed by using the Voigt profile (which is a convolution of Lorentzian and Gaussian) defined as<sup>41</sup>

$$V(\omega) = \frac{\left[ \int_{-\infty}^{+\infty} \frac{a_{Vgt} \exp(-x^2) dx}{\Gamma_{VL}^2 + \left[ \frac{\omega - \omega_{Vgt}}{\Gamma_{VG}} - x \right]^2} \right]}{\int_{-\infty}^{+\infty} \frac{\exp(-x^2) dx}{\Gamma_{VL}^2 + x^2}} \quad (2)$$

where  $a_{Vgt}$  and  $\omega_{Vgt}$  are the amplitude and the center of the distribution, respectively;  $\Gamma_{VG}$  is a width related to the Gaussian half width at half-maximum ( $\Gamma_G = \Gamma_{VG}(2 \ln 2)^{1/2}$ ); and  $\Gamma_{VL}$  is a width depending on the ratio of the Lorentzian half width at half-maximum to  $\Gamma_{VG}$  ( $\Gamma_L = \Gamma_{VG}\Gamma_{VL}$ ). The statistical parameters were used as a guide to a best fit.

## RESULTS

**A. PPG–Water Binary System.** *A.1. Calorimetric Studies.* A first characterization of the samples was done by means of DSC, to analyze the thermal behavior of the sample as a function of water concentration. The maximum water concentration in PPG–water mixtures was  $x_w = 0.40$ , to avoid any possible crystallization of the sample under the cooling experimental conditions. A typical DSC curve showing the heat flow of the PPG–water mixture with  $x_w = 0.40$  during cooling and heating (at a rate of 10 K/min) is depicted in Figure 1. It is evident that it

is possible to avoid crystallization during cooling to obtain a glassy state at low temperatures. However, the heating curve drawn in Figure 1 shows a glass transition ( $T_g$ ) followed by a cold crystallization in the temperature range 220–245 K and the melting in the range between 245 and 265 K. The  $T_g$ 's of all the samples were determined as the onset of the heat flow step, and values are tabulated in Table 1.

**A.2. Dielectric Studies.** Dry PPGs of different molecular weights have been studied previously by several researchers with various techniques.<sup>42–49</sup> However, since our sample could differ from those, it was necessary to measure the dielectric behavior of the dry sample so that a precise comparison with the water mixtures could be made. Therefore, first of all, we have done the dielectric measurement on a dry PPG sample. It is important to note that some water molecules can still remain in our “dry-PPG”. However, as we will see below, these water molecules cannot be detected by broadband dielectric spectroscopy (BDS). From this point of view, our “dry” sample is a good reference for the present comparative study. In the rest of the paper, we will call this sample dry-PPG even if the water content is not strictly zero. The dielectric loss spectra ( $\epsilon''(\omega)$ ) of dry PPG exhibit two well-resolved secondary relaxation processes (designated as  $\beta$  and  $\gamma$  processes) at temperatures lower than  $T_g$  in addition to the main relaxation process ( $\alpha$  process). The dielectric strength of the  $\beta$ -process, which emerges from the excess wing on the high-frequency side of the primary relaxation process, is the smallest. The  $\gamma$ -process is clearly visible in the vicinity of glass transition temperature ( $T_g$ ) and becomes better resolved in the glassy state. The loss peak corresponding to the  $\gamma$ -process is broad and less intensive in comparison to the  $\alpha$ -process. [It is worth mentioning that the  $\gamma$ -process becomes asymmetric in the glassy state, and therefore we have applied the HN function to the best fit of the  $\gamma$ -process]. However, the  $\beta$  process is well described by the Cole–Cole function in the whole temperature range. That agrees also with those observed by Grzybowska et al.<sup>43,44</sup> for 3PG and PPG-400 in their dielectric measurement at ambient pressure.

After confirming and describing the dielectric behavior of the dry PPG sample, dielectric measurements were performed on the PPG–water binary system. Depicted in Figure 2 are dielectric loss for PPG–water mixtures ( $x_w = 0.10$  and 0.30) at various temperatures. In this concentration range, the  $\alpha$ -relaxation of the system becomes faster when increasing water content as usual for other water solutions.<sup>18</sup> From this figure, it is also clear that even a small amount of water has a visible influence on the dielectric loss spectra. At low water concentration (i.e., at  $x_w = 0.10$ ), it can be noticed that below the glass transition temperature a new additional relaxation process (designated as process II) appears. This new relaxation process is located in between the main  $\alpha$ - and  $\gamma$ -relaxations. From a closer examination of the dielectric

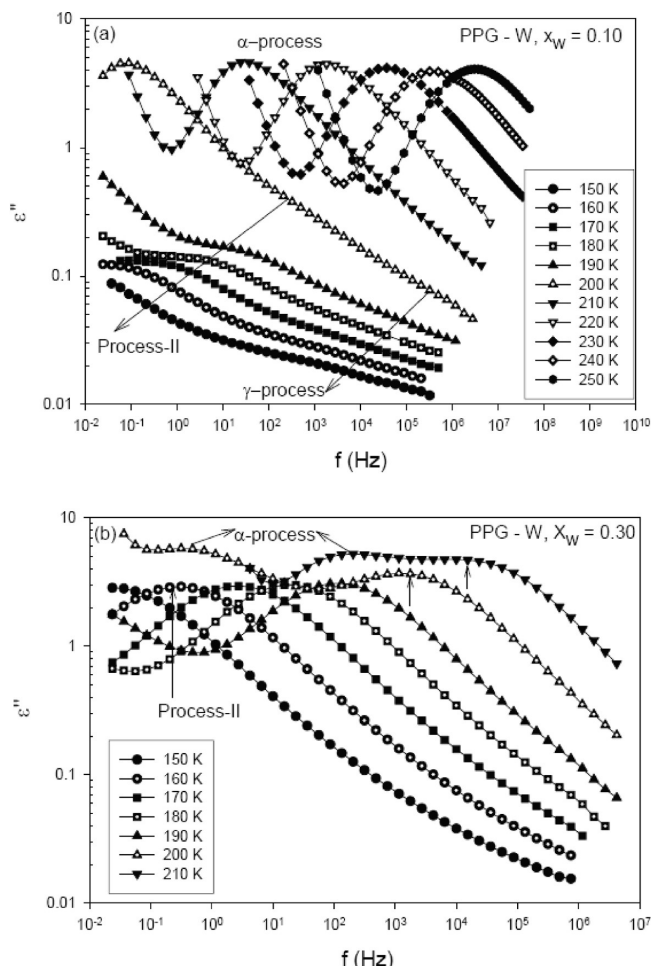


**Figure 2.** Dielectric loss ( $\epsilon''$ ) curves of PPG–water solutions with water concentrations of (a)  $x_w = 0.10$  and (b)  $X_w = 0.30$  at several temperatures.

loss spectra shown in Figure 2(a) and 2(b), one can note the increase of strength of process II with increasing water concentration. Because of the presence of this process,  $\gamma$ -relaxation (which is a clear process in the dry sample) becomes hardly resolved or even almost undetectable at high hydration level ( $x_w \geq 0.20$ ). Figure 3(a) and 3(b) shows examples of the fitting procedure for  $x_w = 0.10$  and 0.30 of PPG–water solutions at 160 and 200 K, respectively. The dielectric loss spectra for low water concentrations ( $x_w = 0.02$  and 0.10) and low temperatures can be described by the sum of two Cole–Cole functions [see Figure 3(a)], whereas at higher  $x_w$  only one Cole–Cole is necessary to fit the spectrum because process II masks the presence of  $\gamma$ -relaxation.

The temperature dependence of the relaxation time  $\tau$  is shown in Figure 4(a–c) for dry PPG and a series of PPG–water solutions. The temperature dependence of the  $\alpha$ -relaxation time data for dry PPG is well described by a Vogel–Fulcher–Tamman (VFT)<sup>21</sup> relation,  $\tau(T) = \tau_0 e^{(B/(T-T_0))}$  where  $B = DT_0$  and  $D$  is related to the fragility index  $m$  and  $\tau_0$  is a pre-exponential factor. Values of these parameters are shown in Table 1 and agree well with previous reports on PPG.<sup>42–44</sup> By extrapolating this equation to a relaxation time of  $\approx 100$  s, a dielectric estimation of the glass transition temperatures ( $T_{g,100s}$ ) of PPG–water solutions is obtained.  $T_{g,100s}$  correlates well with the glass transition temperatures observed by DSC of the PPG–water binary

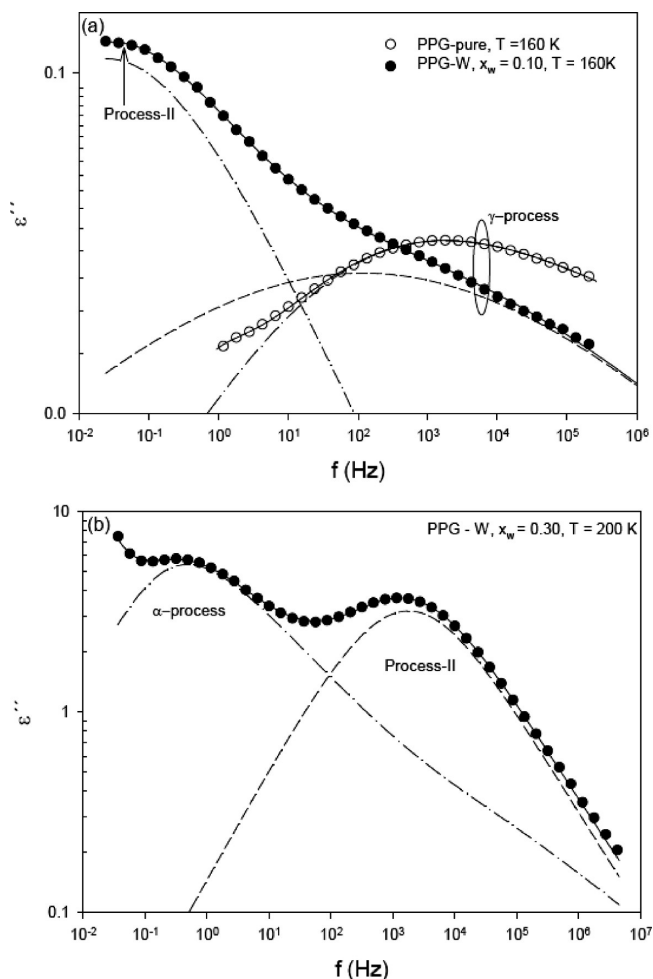


**Figure 3.** (a) Comparison of loss spectra of pure PPG and PPG–water solution with  $x_w = 0.10$  at a fixed temperature. The solid line in the case  $x_w = 0.10$  denotes the fit based on the superposition of two CC functions (dashed and dashed dotted lines), whereas the dashed dotted line for pure PPG represents the fitted curve by the HN function. (b) Dielectric spectrum for  $x_w = 0.30$  of the PPG–water solution at 200 K. The solid line is a least-squares fit using a superposition of a power law for conductivity (not shown), the imaginary part of a HN function (dashed dotted line) for  $\alpha$ -process, and the imaginary part of a CC function (dashed line) for process II.

system, and therefore the dielectric relaxation we are observing ( $\alpha$ -process) corresponds to the structural relaxation of this binary system. To characterize the deviations from the Arrhenius equation of the main relaxation process ( $\alpha$ -process), we calculated the dynamic fragility index ( $m$ ) as<sup>50,51</sup>

$$m = \frac{d(\log \tau)}{d(T_g/T)} \Big|_{T=T_{g,100s}} \quad (3)$$

which indicates the steepness of the evolution of the relaxation time (or viscosity) as a function of  $T$  near to  $T_g$  for each weight fraction. Generally, it ranges from a lowest limiting value of 16 for strong glasses to values as large as 191 for very fragile glasses as poly(vinyl chloride).<sup>50</sup> In the present case, the calculated fragility parameters  $m$  vary from 71.5 to 87.6. Hence, the fragile character slightly increases with increasing water concentration in PPG.

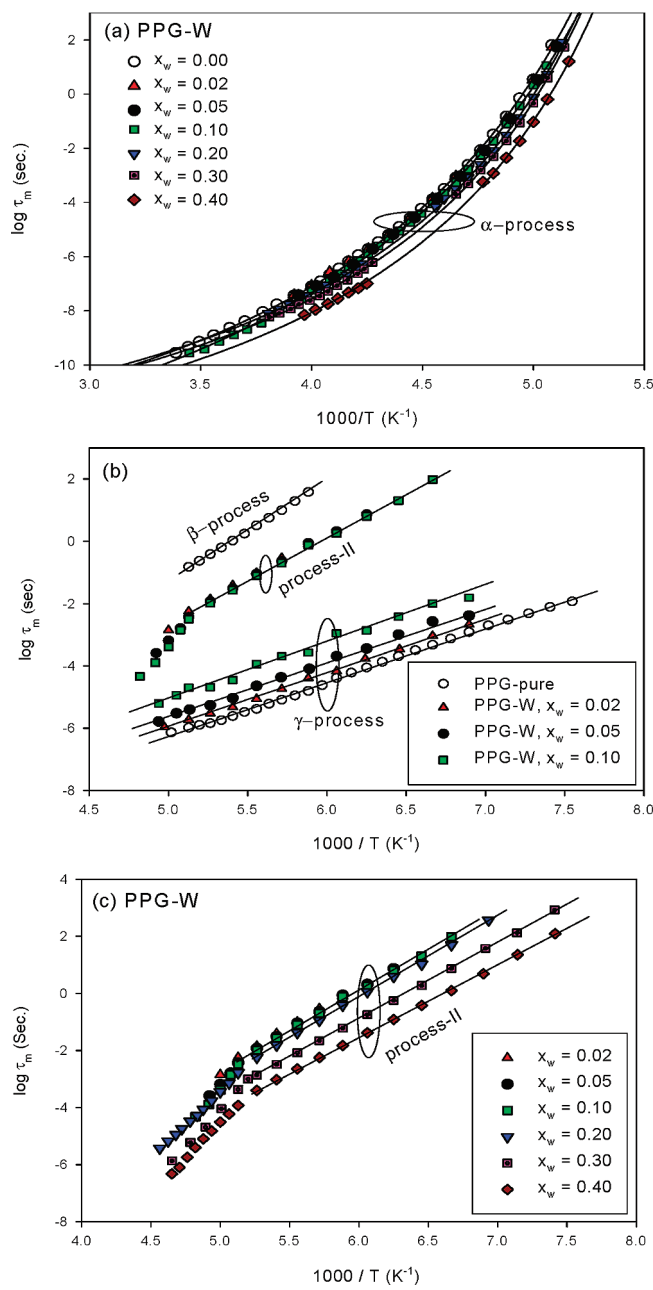


**Figure 4.** Temperature dependence of the relaxation times for PPG–water solutions corresponding to (a)  $\alpha$ -relaxation, (b) process II, and (c) process III only at low water concentration. In (a) the lines along the  $\alpha$ -process are fits to the VFT equation (eq 3). In both (b) and (c), the lines along the process II and  $\gamma$ -process are fits to the Arrhenius equation (eq 4).

Focusing on the relaxation times of the solutions (Figure 4b), we have to mention that process II (associated to the orientation of water molecules) exhibits a crossover from non-Arrhenius to Arrhenius temperature behavior at  $T_g$  of the whole system (see Figure 5). This crossover is rather sharp as compared with other systems.<sup>17,19,29</sup> A representative result is shown in Figure 5 together with the heating DSC curve for the same solution ( $x_w = 0.4$ ). From this figure, it is clear that the relaxation times of process II change from high-temperature VFT to low-temperature Arrhenius around the glass transition determined by DSC.

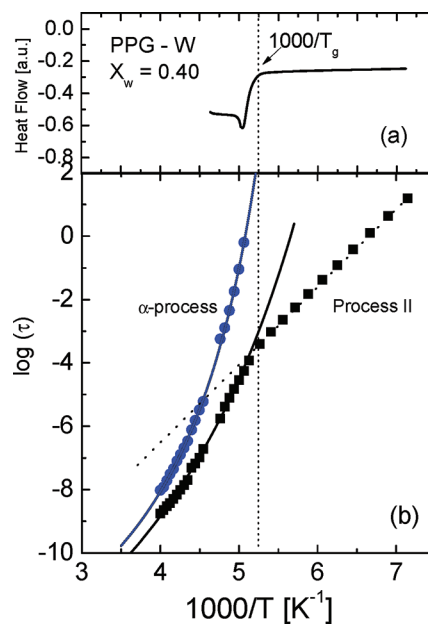


**Figure 5.** (a) Heat flow measured by DSC of the PPG–water solution with  $x_w = 0.40$ , during heating at a rate of 10 K/min. (b) The corresponding temperature dependence of the relaxation times obtained from dielectric spectroscopy of PPG–water solution. A crossover is observed when the system reaches the calorimetric  $T_g$ . Solid lines correspond to the Vogel–Fulcher–Tamman equation to  $\alpha$ -relaxation and process II, respectively, whereas the dotted line corresponds to the Arrhenius equation.

**Table 2. Details of Equation 4 for Process II of the PPG–Water Binary System**

weight fraction of water ( $x_w$ )	$\log \tau_o$ [s]	$E_A$ [eV]
0.02	-17.9	$0.60 \pm 0.01$
0.05	-17.2	$0.57 \pm 0.01$
0.10	-16.5	$0.56 \pm 0.01$
0.20	-17.6	$0.55 \pm 0.01$
0.30	-16.7	$0.52 \pm 0.01$
0.40	-16.2	$0.49 \pm 0.01$

The fitting values of the VFT equation corresponding to the high-temperature range were:  $B = 883.9$  K,  $T_0 = 155.9$  K, and  $\log(\tau_0) = -12.8$ .

Below  $T_g$ , the relaxation times of process II and  $\gamma$  relaxations were described by the well-known Arrhenius equation

$$\tau(T) = \tau_{\text{ARR}} \exp(E_A/RT) \quad (4)$$

where  $\tau_{\text{ARR}}$  is a pre-exponential factor;  $R$  is a gas constant; and  $E_A$  is the apparent molar activation energy. The Arrhenius fit parameters of PPG–water solutions are collected in Tables 2 and 3. The activation energies of process II and  $\gamma$ -process change weakly with the water concentration (see Tables 2 and 3).

Finally, Figure 6 shows the dielectric strength of  $\alpha$ -relaxation and process II as a function of water concentration. The dielectric strength of the  $\alpha$ -process ( $\Delta\epsilon_\alpha$ ) increases with increasing water concentration up to  $x_w = 0.20$  and then starts decreasing smoothly. Conversely, the dielectric strength of process II ( $\Delta\epsilon_{\text{II}}$ ) increases with water concentration over the explored range, but above  $x_w \geq 0.20$ ,

**Table 3. Details of Equation 4 for the  $\gamma$ -Process of the PPG–Water Binary System**

weight fraction of water ( $x_w$ )	$\log \tau_o$ [s]	$E_A$ [eV]
0.00	−15.01	$0.35 \pm 0.01$
<0.02	−14.68	$0.34 \pm 0.01$
0.05	−14.62	$0.34 \pm 0.01$
0.10	−13.94	$0.34 \pm 0.01$

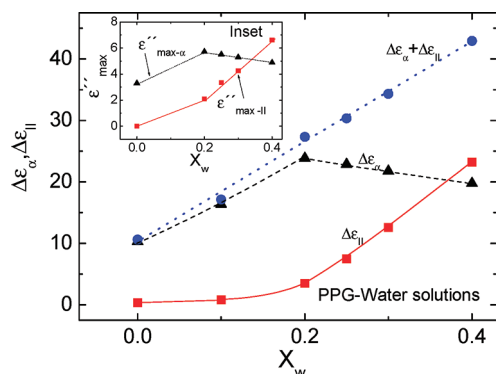


**Figure 6.** Variation of the dielectric strength ( $\Delta\epsilon$ ) versus water concentration ( $x_w$ ) for the PPG–water mixture: for process I at 205 K and process II at 175 K. Inset: maximum value of the dielectric loss versus water concentration.

$\Delta\epsilon_{II}$  increases much more rapidly than at lower water concentration. At the highest water concentration,  $\Delta\epsilon_{II}$  is even greater than the relaxation strength ( $\Delta\epsilon_\alpha$ ) of the  $\alpha$ -process, indicating an increase in the water mobility likely related with the appearance of water domains. In addition, Figure 6 also shows the total relaxation strength ( $\Delta\epsilon_\alpha + \Delta\epsilon_{II}$ ) which increases with increasing  $x_w$  as expected because of the high dipole moment of water molecules. Finally, we note that the variation of  $\Delta\epsilon_\alpha$  with concentration does not follow the “normal” behavior of other multicomponent systems without interactions. To confirm the result obtained by the fitting procedure, the maximum value of the dielectric loss peak was considered. The inset of Figure 6 shows this value (taken directly from the data) as a function of water concentration. We can observe that the intensity of both relaxation processes reflects the same concentration dependence as shown in Figure 6 obtained from the fitting procedure.

**A.3. FTIR-ATR Studies.** Depicted in Figure 7(a) and (b) are the IR absorption spectra of dry PPG, in the wavenumber range  $3700$ – $2800$   $\text{cm}^{-1}$ , below and above the glass transition temperature, respectively. This absorption spectrum consists of O–H stretching modes between  $3700$  and  $3000$   $\text{cm}^{-1}$  and CH-stretching vibrations between  $3000$  and  $2800$   $\text{cm}^{-1}$ . From this figure, it is clear that peak positions at  $2970$ ,  $2930$ , and  $2870$   $\text{cm}^{-1}$  (corresponding to CH-stretching vibrations) are not affected by varying the temperature, but the intensity decreases with increasing temperature. In addition, the temperature dependence of IR absorption spectra for the OH-stretching vibration (in the range of  $3600$ – $3000$   $\text{cm}^{-1}$ ) shows two different kinds of behavior depending on the temperature range. Below  $T_g$ , the spectra of the OH-stretching region are more or less unchanged [see Figure 7(a)]; however, above  $T_g$ , as the temperature increases, the OH-stretching band shifts to higher frequencies ( $3385$ – $3435$   $\text{cm}^{-1}$ ) while the intensity decreases [see Figure 7(b)]. This tendency may be due to the fact that the

peak position of the IR absorption band essentially represents the degree of restriction of the vibrational motion of the chemical bond, which is almost dependent on the extent of interactions with other groups. Therefore, the shift of the absorption spectra of the OH-stretching band toward the higher wavenumber with increasing temperature clearly indicates that the thermal energy decreases the extent of formation of hydrogen bonds between hydroxyl groups.

Since our main interest is to see how the OH-stretching region is affected by the presence of water, we have done the detailed analysis of the OH-stretching region at different temperatures by following the scheme given by Crupi<sup>41</sup> et al. Accordingly, we identify the vibration found in PPG near  $3500$   $\text{cm}^{-1}$  as the fundamental OH-stretching mode of end and (or) open monomer group. The band at  $3400$   $\text{cm}^{-1}$  represents the OH-stretching vibrations in which the oxygen or hydrogen atom of one molecule makes a bond with another hydrogen or oxygen atom of another molecule forming a dimer. Finally, the third band near  $3300$   $\text{cm}^{-1}$  shows the existence of intramolecular stretching vibration in which both the hydrogen and oxygen atom of one unit are involved in intermolecular hydrogen bonding with the nearest units making trimers or more extended structures. Two representative examples (below and above  $T_g$ ) of the fitting procedure adopted are shown in the inset of Figure 7(a) and (b). The corresponding area of these bands as a function of temperature is plotted in Figure 7(c). The area of all three bands is almost constant with respect to the temperature; however, one can see a slight jump at the glass transition temperature.

After accessing the FTIR-ATR results of dry PPG, we have done FTIR-ATR measurements on PPG–water solutions. One representative example of IR absorption spectra of the PPG–water solution for  $x_w = 0.30$  at different temperatures is shown in Figure 8(a). The intensity of the OH-stretching band decreases with increasing temperature, and peak positions slightly shift to higher wavenumbers. It is important to note that the IR data of the solutions cannot be described just by a linear combination of the pure components due to the interaction between the two components. The area of the OH-stretching region is well described by eq 2 using three bands centered at around  $3200$ ,  $3400$ , and  $3500$   $\text{cm}^{-1}$  as can be seen in Figure 8(b) at  $T = 153$  K. The intensities as a function of temperature are depicted in Figure 8(c). Note that in the Supporting Information we show the variation of the peak positions with temperature during fitting. The intensity of the band centered at  $3200$   $\text{cm}^{-1}$  decreases with an increase in temperature, while other bands centered at around  $3400$  and  $3500$   $\text{cm}^{-1}$  are almost constant in the whole temperature range.

## DISCUSSION

As water molecules are added to the dry PPG, the  $T_g$  value remains almost constant at very low water concentrations ( $0.02 < x_w < 0.1$ ) and then clearly decreases. This fact indicates that at low water concentration water molecules have no strong impact on the motion of PPG molecules, whereas at higher water concentrations water molecules facilitate the motion of PPG acting like a plasticizer. This is the “normal” behavior for several glass forming systems, but some authors have reported an increase in  $T_g$  values for low to moderate water concentration in propylene glycol monomethyl ether (PGME).<sup>20</sup>

In addition to the  $\alpha$ -relaxation, dry PPG exhibits two secondary relaxations ( $\beta$  and  $\gamma$ ). When PPG is hydrated,  $\beta$ -relaxation is

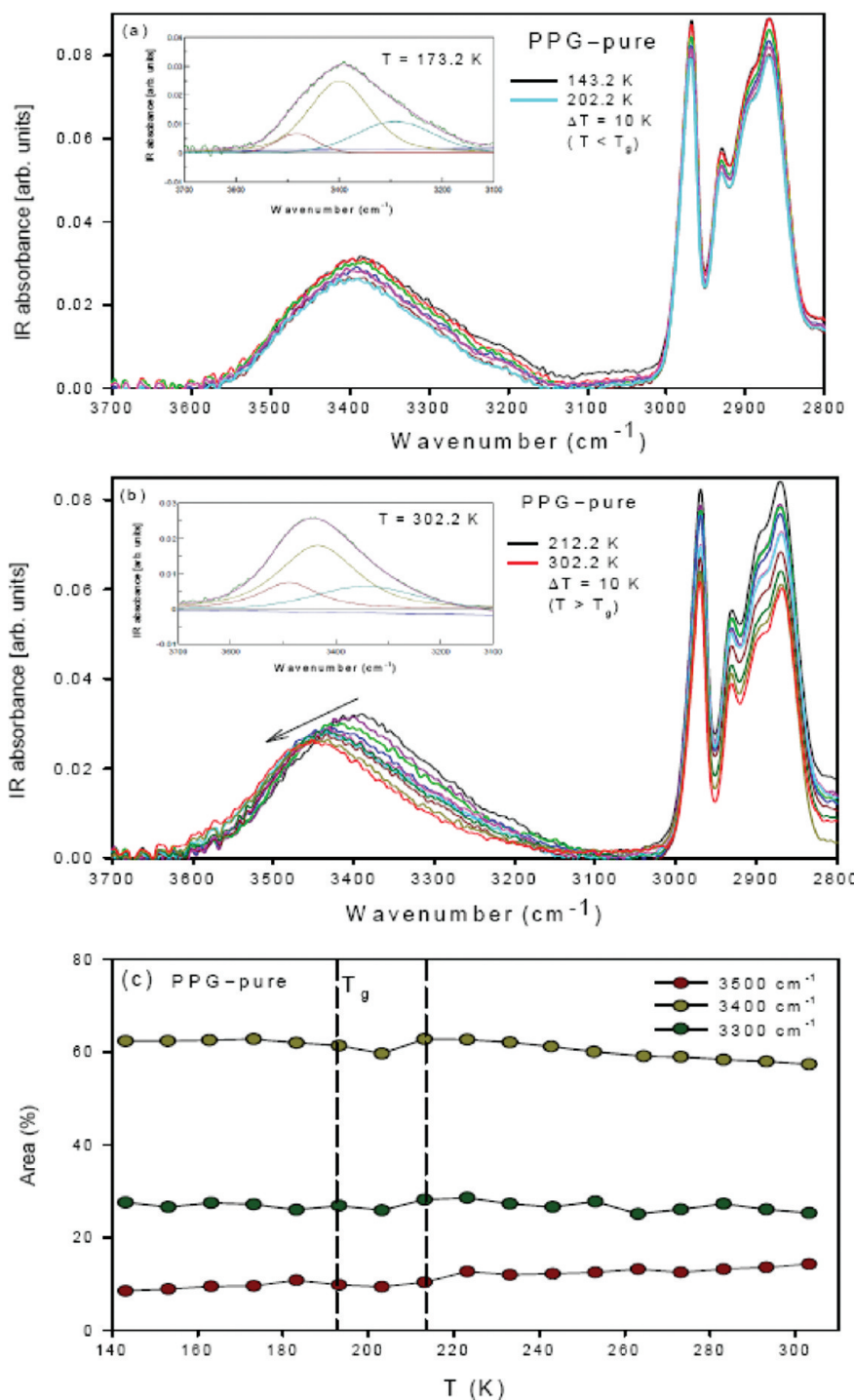


**Figure 7.** ATR-FTIR: Evolution of OH- and CH-stretching bands of pure PPG with respect to temperature (a) below the glass transition temperature ( $T \leq T_g$ ) and (b) above the glass transition temperature ( $T \geq T_g$ ). Inset: the least-squares fit of the  $-OH$  stretching region of the pure PPG sample, obtained using three Voigt profiles (eq 2). Panel (c) shows the variation of areas of the  $-OH$  stretching sub-bands centered between 3700 and  $3000\text{ cm}^{-1}$  for pure PPG as a function of temperature.

undetectable because its relaxation strength is lower by more than 1 order of magnitude than that of water molecules, and it appears in the same frequency range. For this reason, we cannot further study the influence of water molecules on this relaxation. However,  $\gamma$ -relaxation is well resolved up to water concentrations of  $x_w = 0.10$ . The relaxation times corresponding to this process become larger with increasing water concentration,

although the activation energy remains constant (0.34 eV). In spite of the fact that we do not know the molecular origin of  $\gamma$ -relaxation, we can notice that water molecules seem to hamper this relaxation. Therefore, we can speculate that this relaxation seems to be caused by some partial or full rotations of molecular units containing  $-OH$  groups interacting with water molecules.

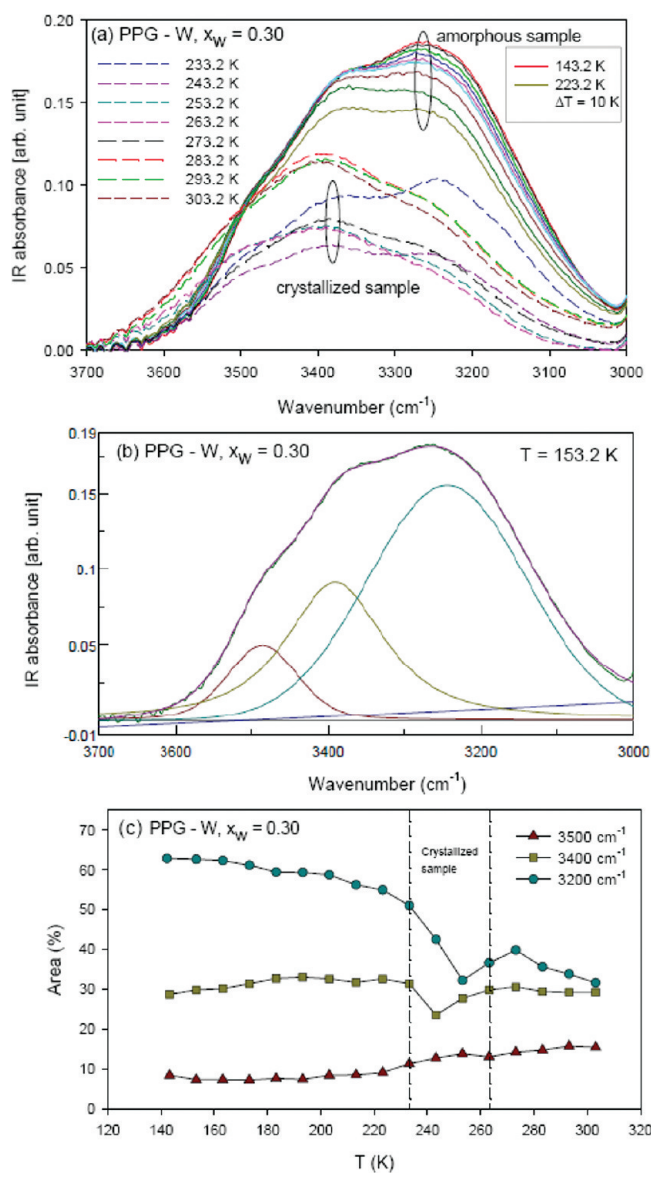


**Figure 8.** ATR-FTIR: (a) Evolution of OH-stretching band versus temperature (during heating) for PPG–water solution with  $x_w = 0.30$ . (b) The least-squares fit of the –OH stretching region of PPG–water solution at a fixed temperature, obtained using three Voigt profiles (eq 2). Panel (c) show the corresponding variation of areas of the –OH stretching sub-bands centered between 3700 and 3000  $\text{cm}^{-1}$  as a function of temperature.

In the following, we focus mainly on the behavior of the water relaxation (process II). As water is added to PPG, the relaxation strength of this process ( $\Delta\epsilon_{II}$ ) systematically increases with water content confirming that water molecules are responsible for this relaxation (see Figure 6). This observation agrees well with dielectric data in other water solutions (for instance, glycerol, poly(vinyl methyl ether) (PVME), poly(vinyl pyrrolidone) (PVP), propylene glycol oligomers, and ethylene glycol oligomers<sup>16–19</sup>). As previously mentioned, the relaxation times for this process show two different behaviors depending on the temperature range [see Figure 4(c) and 5]. Below  $T_g$  it follows an Arrhenius temperature dependence, whereas above  $T_g$  the behavior changes (see Figure 5). From this fact, earlier researchers have suggested that this crossover is related

to the fragile-to-strong transition proposed by Ito et al.<sup>52</sup> for bulk water. However, from the results presented here and elsewhere,<sup>3,17,53</sup> we can observe that the crossover temperature can be identified with the freezing-in of the mixture at the glass transition temperature. Below the calorimetric glass transition, water molecules are moving inside a rigid environment (the frozen PPG), whereas above the glass transition of the mixture the polymer matrix is mobile and the water molecular dynamics occurs in a highly fluctuating environment. In this situation, the temperature dependence of the relaxation times would follow VFT temperature dependence, as illustrated in Figure 5 by means of a solid line. In addition, Swenson and collaborators<sup>54–57</sup> have suggested that the low-temperature Arrhenius behavior is due to a  $\beta$ -like relaxation process of the supercooled water, and therefore the crossover is a result of a merging of this secondary process with the cooperative  $\alpha$ -relaxation of water molecules which, for some reason, is nonobservable with dielectric spectroscopy. In the two explanations, the “Arrhenius part” is seen as a local relaxation process of water molecules. During cooling when the system reaches  $T_g$ , the overall structure becomes frozen, but water molecules move confined by other water molecules.

We have to mention that the VFT parameters (at  $T > T_g$ ) corresponding to  $\alpha$ -relaxation and process II showed that both relaxations are not parallel to each other, but they are in some way coupled (because the  $T_0$  value can be fixed to be the same for both relaxations). This suggests that, approaching  $T_g$ , both relaxations are coupled to the structural molecular motions, and process II would preferentially probe the fast part of the global relaxation. In addition, at low temperature the water relaxation times become faster with increasing water content, and the activation energy decreases (see Table 2). This behavior is similar<sup>18</sup> to that observed in water solutions of nPG oligomers ( $n = 1, 2$ , or 3) but different from that observed in solutions of more “rigid” systems like PVME<sup>17</sup> or PVP<sup>19</sup> where the times become faster but the activation energy systematically increases with water concentration. However, at the highest water concentration all the different systems seem to present a water relaxation with similar average activation energy ( $\sim 0.5$  eV) independent of the interaction details between water and solute molecules.<sup>3</sup>

To explain the behavior of relaxation processes in this binary system, let us apply the Sudo approach.<sup>57</sup> According to this approach, the behavior of relaxation processes can be interpreted by assuming the existence of three types of cooperative domains (CDs) containing: (i) only PPG molecules (CD<sub>PPG</sub>), (ii) only water molecules (CD<sub>W</sub>), and (iii) both PPG and water molecules, bounded by hydrogen bonds (CD<sub>PPG-W</sub>). The data analysis of the PPG–W solutions suggests two characteristic regions below and above  $x_w = 0.20$ . The first region contains two kinds of domains, CD<sub>PPG</sub> and CD<sub>PPG-W</sub>, and the probability of the existence of clusters of water molecules (CD<sub>W</sub>) is very small. The second region includes mainly two kinds of domains, CD<sub>PPG-W</sub> and CD<sub>W</sub>, whereas clusters of PPG molecules (CD<sub>PPG</sub>) are less probable. When a small amount of water is mixed with pure PPG, water molecules destroy some clusters of PPG while forming the hydrogen-bonded mixed network of PPG and water molecules. This implies that the formation of CD<sub>PPG-W</sub> besides CD<sub>PPG</sub> already existing in pure PPG. This change in structure corresponds to the appearance of a new relaxation process (process II) with the small dielectric strength. Therefore, the origin of process II at  $x_w < 0.20$  can be explained

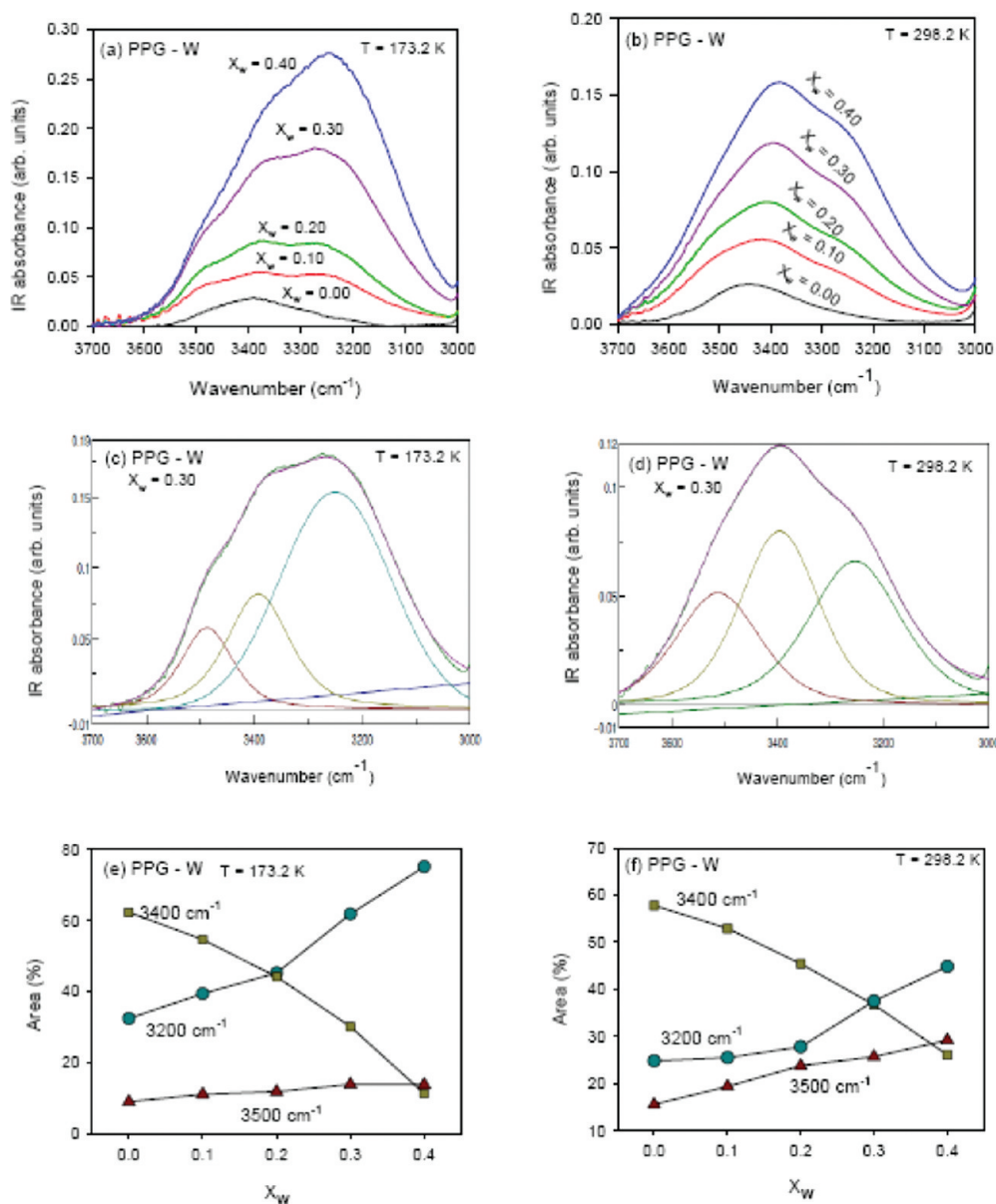


**Figure 9.** ATR-FTIR: Evolution of OH-stretching region with changing water concentration in PPG solution: (a) at 173.2 K and (b) at 298.2 K. Panels (c) and (d) show the least-squares fit of the PPG–water solutions at  $x_w = 0.30$ , obtained using three Voigt profiles at 173.2 and 298.2 K, respectively. Panels (e) and (f) show the corresponding variation of areas of OH-stretching sub-bands centered between 3700 and 3000  $\text{cm}^{-1}$  for PPG–water mixtures as a function of water concentration.

by local reorientations of water molecules incorporated in the hydrogen bonding network of PPG. The dielectric loss spectra for the  $\alpha$ -relaxation asymmetrically broaden after addition of water. This fact may be due to the presence of more heterogeneous distributions because water is more “flexible” than PPG and larger variations of  $\text{CD}_{\text{PPG-W}}$  sizes in comparison with  $\text{CD}_{\text{PPG}}$  sizes. Therefore, both  $\text{CD}_{\text{PPG}}$  and  $\text{CD}_{\text{PPG-W}}$  mainly contribute to the  $\alpha$ -relaxation. Accordingly, one can notice that the  $\alpha$ -relaxation dielectric strength increases with increasing water concentration in PPG–W solutions up to  $x_w = 0.20$  where it reaches its maximum value (see Figure 6). On increasing the concentration of water in the mixture, the fraction of  $\text{CD}_{\text{PPG-W}}$  becomes larger, whereas the fraction of  $\text{CD}_{\text{PPG}}$  decreases. Then, some molecules of PPG are fully or partially surrounded by water molecules and can more easily rotate cooperatively than in the

PPG cluster. Hence, the relaxation time of  $\alpha$ -relaxation becomes smaller. Above  $x_w = 0.20$  the  $\text{CD}_w$  domains are created and critically influence the dynamics of the mixture. Further addition of water causes the increase of the  $\text{CD}_w$  fraction and the decrease of the  $\text{CD}_{\text{PPG-W}}$  fraction [see Figure 2(b)]. A formation of homogeneous clusters of PPG is improbable in this case. At  $x_w > 0.20$  the contribution of the process II to the loss spectra increases and becomes comparable or even larger than the  $\alpha$ -relaxation. The manifestation of such behavior is the drastic change of the dielectric strength of process II with increasing  $x_w$ .

The above results are confirmed when compared with ATR-FTIR measurements of the –OH stretching band, performed on pure PPG and PPG–water solutions in the frequency range  $3000$ – $3800 \text{ cm}^{-1}$  and in the temperature range  $143$ – $302 \text{ K}$ . In Figure 9(a) and 9(b), we have shown the FTIR-ATR spectra of

various water concentrations in PPG at 173.2 and 298.2 K. From this figure, it is clear that the absorption area corresponding to OH-stretching vibrations increases by increasing water concentration. According to previous studies, the OH stretching band of bulk water can be decomposed into three main components<sup>27,30,39</sup> that could be attributed to three types of water species. Fully tetrahedrally coordinated hydrogen-bonded water molecules contribute to the wavenumber at about 3200 cm<sup>-1</sup> and represent the bulklike structure of water or the so-called network water.<sup>30,39</sup> Its appearance in a spectrum is an indication of a high degree of hydrogen bonding order. Weakly hydrogen-bonded water appears at higher frequencies (near 3500 cm<sup>-1</sup>), and it corresponds to small water aggregates or water having no contacts with other water molecules.<sup>30,39</sup> Between these two extremes there are water molecules in an environment of partial hydrogen bond that contribute to the infrared spectra at intermediate frequencies (at about 3400 cm<sup>-1</sup>), and it could reflect the interaction of water molecules with a solute, surface, or a confining environment.<sup>30,32,37,39</sup> Following this scheme, we performed free fits of the —OH stretching band data, as described in the experimental part, using three components in the PPG—water solution, the same as in the case of pure PPG discussed in Section A.3. Two examples (one at 173.2 K and another at 298.2 K) of such fitting procedure are depicted in Figures 9(c) and 9(d), for the PPG—water system at  $x_w = 0.30$ . In particular, for PPG—water solution, three components are necessary to correctly describe the data: the first centered at about 3500 cm<sup>-1</sup>, the second at 3400 cm<sup>-1</sup>, and the third one close to 3200 cm<sup>-1</sup> as mentioned in results Section A.3. Figures 9(e) and 9(f) show the variation of percentage areas with different water concentrations for the three bands obtained from spectral band fitting of the OH-stretching region shown in Figures 9(c) and 9(d). The band at 3200 cm<sup>-1</sup>, attributed to strongly hydrogen bonded water, increases with the increasing water concentration in PPG. However, the variation of area with respect to water concentration is nonlinear. With increasing water concentration, the percentage area of this band increases linearly with a moderate slope up to  $x_w = 0.20$  and then starts to increase more rapidly beyond this critical concentration [see Figures 9(e) and 9(f)]. On the other hand, the percentage area of sub-band at about 3500 cm<sup>-1</sup> slightly increases at a high hydration level, while the percentage area of sub-band at 3400 cm<sup>-1</sup> continuously decreases with increasing concentration of water. From these results, we could argue that the fraction of water molecules directly interacting with the polymer, and contributing to the ATR-FTIR spectra about 3400 cm<sup>-1</sup>, decreases with increasing hydration levels. Conversely, the percentage of strongly hydrogen-bonded water molecules with a full tetrahedral coordination increases with increasing hydration level, more rapidly above  $x_w = 0.20$  [see Figures 9(e) and 9(f)]. It should be noted that the relative abundance of these two species of water reverts with increasing water concentration. That is, water—PPG interacting molecules are predominant at low water concentration, and those water—water strongly hydrogen-bonded molecules dominate at high water concentration, i.e.,  $x_w > 0.20$ . Finally, it is important to note that the slight increase of a third component in the ATR-FTIR spectra at about 3500 cm<sup>-1</sup>, when  $x_w = 0.20$ , suggests that with increasing water concentration in PPG the water behavior in PPG solutions tends to approach that of bulk water, with the FTIR absorbance showing all three characteristic components.

Put together, the BDS and ATR-FTIR data further validate the hypothesis that in PPG—water solutions, above a water content of about  $x_w = 0.20$ , the dynamical behavior of water is dominated mainly by water—water interactions. This conclusion is also

supported by the temperature dependence analysis of process II relaxation times as discussed above [compare Figures 6, 9(e), and 9(f)].

## ■ ASSOCIATED CONTENT

**S Supporting Information.** Additional figures 1 and 2. This material is available free of charge via the Internet at <http://pubs.acs.org>.

## ■ AUTHOR INFORMATION

### Corresponding Author

\*E-mail: scerveny@ehu.es.

## ■ ACKNOWLEDGMENT

The authors gratefully acknowledge the support of the Spanish Ministry of Education (MAT2007-63681) and the Basque Government (IT-436-07).

## ■ REFERENCES

- (1) Stillinger, F. H. *Science* **1980**, *209*, 451.
- (2) Tokmako, A. *Science* **2007**, *317*, 54.
- (3) Cerveny, S.; Alegria, A.; Colmenero, J. *Phys. Rev. E* **2008**, *77*, 031803.
- (4) Mashimo, S.; Miura, N.; Umehara, T. *J. Chem. Phys.* **1992**, *97*, 6759.
- (5) Fuchs, K.; Kaatze, U. *J. Chem. Phys.* **2002**, *116*, 7137.
- (6) Stenger, J.; Cowman, M.; Eggers, F.; Eyring, E. M.; Kaatze, U.; Petrucci, S. *J. Phys. Chem. B* **2000**, *104*, 4782.
- (7) Pagnotta, S. E.; Cerveny, S.; Alegria, A.; Colmenero, J. *J. Chem. Phys.* **2009**, *131*, 085102.
- (8) Shinyaishi, N.; Yamamoto, W.; Yokoyama, A.; Yoshinari, T.; Yagihara, S.; Kita, R.; Ngai, K. L.; Capaccioli, S. *J. Phys. Chem. B* **2009**, *113*, 14448.
- (9) Jansson, H.; Bergman, R.; Swenson, J. *J. Phys. Chem. B* **2005**, *109*, 24134.
- (10) Gainaru, C.; Fillmer, A.; Bohmer, R. *J. Phys. Chem. B* **2009**, *113*, 12628.
- (11) Pagnotta, S. E.; Cerveny, S.; Alegria, A.; Colmenero, J. *Phys. Chem. Chem. Phys.* **2010**, *12*, 10512.
- (12) Grzybowska, K.; Paluch, M.; Grzybowski, A.; Pawlus, S.; Ancherbak, S.; Prevosto, D.; Capaccioli, S. *J. Phys. Chem. Lett.* **2010**, *1*, 1170.
- (13) Tyagi, M.; Murthy, S. S. N. *Carbohydr. Res.* **2006**, *341*, 650.
- (14) Sudo, S.; Tsubotani, S.; Shimomura, M.; Shinyaishi, N. *J. Chem. Phys.* **2004**, *121*, 7332.
- (15) Shinyaishi, N.; Yagihara, S.; Arita, I.; Mashimo, S. *J. Phys. Chem. B* **1998**, *102*, 3249.
- (16) Murthy, S. S. N. *J. Phys. Chem. B* **2000**, *104*, 6955.
- (17) Cerveny, S.; Colmenero, J.; Alegria, A. *Macromolecules* **2005**, *38*, 7056.
- (18) Cerveny, S.; Schwartz, G. A.; Alegria, A.; Bergman, R.; Swenson, J. *J. Chem. Phys.* **2006**, *124*, 194501.
- (19) Cerveny, S.; Alegria, A.; Colmenero, J. *J. Chem. Phys.* **2008**, *128*, 044901.
- (20) Sjostrom, J.; Mattsson, J.; Bergman, R.; Johansson, E.; Josefsson, K.; Svantesson, D.; Swenson, J. *Phys. Chem. Chem. Phys.* **2010**, *12*, 10452.
- (21) Vogel, H. *Phys. Z.* **1921**, *22*, 645. Fulcher, G. S. *J. Am. Chem. Soc.* **1925**, *8*, 789. Tammann, G.; Hesse, G. Z. *Anorg. Allg. Chem.* **1926**, *156*, 245.
- (22) Johari, G. P.; Goldstein, M. *J. Chem. Phys.* **1970**, *53*, 2372.
- (23) Pathmanathan, K.; Johari, G. P. *J. Phys. C: Solid State Phys.* **1985**, *18*, 6535.
- (24) Singh, L. P.; Murthy, S. S. N. *Phys. Chem. Chem. Phys.* **2009**, *11*, 5110.

- (25) Singh, L. P.; Murthy, S. S. N. *J. Chem. Phys.* **2008**, *129*, 094501.  
(26) Singh, L. P.; Murthy, S. S. N. *J. Phys. Chem. B* **2008**, *112*, 2606.  
(27) Crupi, V.; Longo, F.; Majolino, D.; Venuti, V. *J. Chem. Phys.* **2005**, *123*, 154702.  
(28) Sjostrom, J.; Swenson, J.; Bergman, R.; Kittaka, S. *J. Chem. Phys.* **2008**, *128*, 154503.  
(29) Barroso-Bujans, F.; Cerveny, S.; Alegria, A.; Colmenero, J. *J. Phys. Chem. C* **2010**, *114*, 2604.  
(30) Brubach, J. B.; Mermet, A.; Filabozzi, A.; Gershel, A.; Roy, P. *J. Chem. Phys.* **2005**, *122*, 184509.  
(31) Marechal, Y.; Chamel, A. *J. Phys. Chem.* **1996**, *100*, 8551.  
(32) Crupi, V.; Longo, F.; Majolino, D.; Venuti, V. *J. Phys.: Condens. Matter* **2006**, *18*, 3563.  
(33) Kitano, H.; Ichikawa, K.; Ide, M.; Fukuda, M.; Mizuno, W. *Langmuir* **2001**, *17*, 1889.  
(34) Calandra, P.; Caponetti, E.; Martino, D. C.; Angelo, P. D.; Minore, A.; Liveri, V. T. *J. Mol. Struct.* **2000**, *522*, 165.  
(35) Van Alsten, J. G.; Coburn, J. C. *Macromolecules* **1994**, *27*, 3476.  
(36) Sutander, P.; Ahn, D. J.; Frances, E. I. *Macromolecules* **1994**, *27*, 7316.  
(37) Malsam, J.; Aksan, A. *J. Phys. Chem. B* **2010**, *114*, 4238.  
(38) Malsam, J.; Aksan, A. *J. Phys. Chem. B* **2009**, *113*, 6792.  
(39) Reategue, E.; Aksan, A. *J. Phys. Chem. B* **2009**, *113*, 13048.  
(40) Havriliak, S.; Negami, S. *J. Polym. Sci., Part C* **1966**, *14*, 99.  
(41) Crupi, V.; Majolino, D.; Migliardo, P.; Venuti, V. *Mol. Phys.* **2000**, *98*, 1589.  
(42) Grzybowska, K.; Grzybowski, A.; Ziolo, J.; Razoska, S. J.; Paluch, M. *J. Phys.: Condens. Matter* **2007**, *19*, 376105.  
(43) Grzybowska, K.; Grzybowski, A.; Ziolo, J.; Paluch, M.; Capaccioli, S. *J. Chem. Phys.* **2006**, *125*, 044904.  
(44) Grzybowska, K.; Grzybowski, A.; Pawals, S.; Hensel-Bielowka, S.; Paluch, M. *J. Chem. Phys.* **2005**, *123*, 204506.  
(45) Gainaru, C.; Hiller, W.; Bohmer, R. *Macromolecules* **2010**, *43*, 1907.  
(46) Leon, C.; Ngai, K. L.; Roland, C. M. *J. Chem. Phys.* **1999**, *110*, 2323.  
(47) Johari, G. P. *Polymer* **1986**, *27*, 866.  
(48) Capaccioli, S.; Casalini, R.; Lucchesi, M.; Lovicu, G.; Prevosto, D.; Pisignano, D.; Romano, G.; Rolla, P. A. *J. Non-Cryst. Solids* **2002**, *307–310*, 238.  
(49) Ko, J.-H.; Kojima, S. *Phys. Lett. A* **2004**, *321*, 141.  
(50) Bohmer, R.; Ngai, K. L.; Angell, C. A.; Plazek, D. J. *J. Chem. Phys.* **1993**, *99*, 4201.  
(51) Angell, C. A. *Polymer* **1997**, *38*, 6261.  
(52) Ito, K.; Moynihan, C. T.; Angell, C. A. *Nature* **1999**, *398*, 492.  
(53) Cerveny, S.; Alegria, A.; Colmenero, J. *J. Non-Cryst. Solids* **2007**, *47–51*, 4523.  
(54) Swenson, J.; Jansson, H.; Bergman, R. *Phys. Rev. Lett.* **2006**, *96*, 247802.  
(55) Swenson, J.; Jansson, H.; Hedström, J.; Bergman, R. *J. Phys.: Condens. Matter* **2007**, *19*, 205109.  
(56) Jansson, H.; Swenson, J. *Biochim. Biophys. Acta* **2010**, *1804*, 20.  
(57) Jansson, H.; Swenson, J. *Euro. Phys. J. E* **2003**, *12*, S51.  
(58) Sudo, S.; Shimomura, M.; Shinyashiki, N.; Yagihara, S. *J. Non-Cryst. Solids* **2002**, *307–310*, 356.